

Boosting Semi-Supervised 2D Human Pose Estimation by Revisiting Data Augmentation and Consistency Training

Huayi Zhou¹, Mukun Luo¹, Fei Jiang², Yue Ding¹, and Hongtao Lu¹

¹ Shanghai Jiao Tong University, Shanghai, China

² Chongqing Academy of Science and Technology, Chongqing, China
{sjtu_zhy,luomukun,dingyue,htlu}@sjtu.edu.cn, fjiang@mail.ecnu.edu.cn

Abstract. The 2D human pose estimation (HPE) is a basic visual problem. However, its supervised learning requires massive keypoint labels, which is labor-intensive to collect. Thus, we aim at boosting a pose estimator by excavating extra unlabeled data with semi-supervised learning (SSL). Most previous SSHPE methods are consistency-based and strive to maintain consistent outputs for differently augmented inputs. Under this genre, we find that SSHPE can be boosted from two cores: advanced data augmentations and concise consistency training ways. Specifically, for the first core, we discover the synergistic effects of existing augmentations, and reveal novel paradigms for conveniently producing new superior HPE-oriented augmentations which can more effectively add noise on unlabeled samples. We can therefore establish paired easy-hard augmentations with larger difficulty gaps. For the second core, we propose to repeatedly augment unlabeled images with diverse hard augmentations, and generate multi-path predictions sequentially for optimizing multi-losses in a single network. This simple and compact design is interpretable, and easily benefits from newly found augmentations. Comparing to SOTA approaches, our method brings substantial improvements on public datasets. Code is in <https://github.com/hnuzhy/MultiAugs>

Keywords: Semi-supervised learning · Human pose estimation · Data augmentation · Consistency training

1 Introduction

2D human pose estimation (HPE) aims to detect and represent human parts as sparse 2D keypoint locations in RGB images. It is the basis of many visual tasks such as action recognition [13, 61], person re-identification [46, 71] and 3D human shape regression [41, 42]. Modern data-driven HPE has been substantially improved by generous deep supervised learning approaches [4, 9, 35, 49, 55, 59, 63]. This greatly benefits from the collection and annotation of many large-scale public HPE datasets [1, 29, 34, 53]. However, compared to image classification and detection tasks requiring plain labels, obtaining accurate 2D keypoints from massive images is laborious and time-consuming. To this end, some researches [23, 37, 51, 58] try to alleviate this problem by introducing the semi-supervised

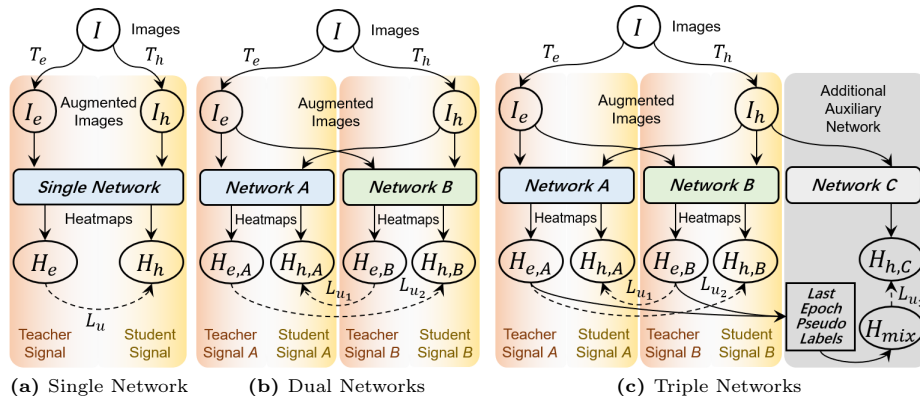


Fig. 1: Frameworks of existing SSHPE methods including Single-Network (a) and Dual-Network (b) proposed by [58], Triple-Network (c) proposed by [23].

2D human pose estimation (SSHPE), which can subtly leverage extensive easier obtainable yet unlabeled 2D human images in addition to partial labeled data to improve performance. Although methods [23, 58] have improved the accuracy of SSHPE task, they overlooked two fundamental questions:

Q1: How to judge the discrepancy of unsupervised data augmentations with different difficulty levels? In [58], as shown in Fig. 1a, for a batch of unlabeled images \mathbf{I} , its easy augmentation \mathbf{I}_e and hard augmentation \mathbf{I}_h are generated separately. Then, predicted heatmap \mathbf{H}_e of \mathbf{I}_e is used as a pseudo label to teach the network to learn the harder counterpart \mathbf{I}_h with its yielded heatmap \mathbf{H}_h . [58] finds that the large gap between two augmentations ($\mathbf{I}_e, \mathbf{I}_h$) matters. Essentially, this is a pursuit for more advanced data augmentations in SSHPE. To rank augmentations of different difficulty levels, [58] observes precision degradation of a pretrained model by testing it on a dataset after corresponding augmentation. However, we declare that this manner is not rigorous. An obvious counter-case is that over-augmented samples approaching noise will get worst evaluation results, but such hard augmentations are meaningless. Contrastingly, we deem that a persuasive ranking requires independent training for each augmentation. We answer this question in detail in Sec. 3.1.

Q2: How to generate multiple unsupervised signals for consistency training efficiently and concisely? Previous work [58] proposes to use a Single-Network to perform the unsupervised consistency training on the easy-hard pair ($\mathbf{I}_e, \mathbf{I}_h$). It also gives a more complicated Dual-Network as in Fig. 1b for cross-training of two easy-hard pairs. SSPCM [23] even constructs a Triple-Network as in Fig. 1c for interactive training of three easy-hard pairs. This pattern of adding more networks with the increase of unsupervised signal pairs can certainly bring gains. But this is cumbersome and will decelerate the training speed proportionally. In practice, considering that augmentations are always performed on the same input, we can repeatedly augment \mathbf{I} multiple times with n diverse hard augmentations, and generate multi-path easy-hard pairs $\{(\mathbf{I}_e, \mathbf{I}_{h_1}), (\mathbf{I}_e, \mathbf{I}_{h_2}), \dots, (\mathbf{I}_e, \mathbf{I}_{h_n})\}$. In this way, we can use only one single network

(refer Fig. 7a) to optimize n pairs of losses. This is also applicable to dual networks (refer Fig. 7b). We discuss this question in detail in Sec. 3.2.

In this paper, we mainly revisit Q1 and Q2 to boost SSHPE. For Q1, after properly ranking existing basic augmentations [10–12, 66, 70], we naturally try to extend it to discover new strong augmentations through reasonable sequential combinations inspired by the AutoAug families [10, 18, 33, 72]. Rather than trivial enumeration, we notice the **synergistic effects** between different augmentations, and reveal novel paradigms for easily generating superior combinations. Our paradigms for the SSHPE task contain three principles: (P1) *Do not combine MixUp-related augmentations.* (P2) *Try to utilize the synergistic effects.* (P3) *Do not over-combine too many augmentations.* These principles have favorable interpretability, and bypass painstaking designs in other advanced augmentations [17, 21, 36, 38, 43, 72]. For Q2, we quantitatively validated the superiority of multi-path design over commonly used heatmaps fusion [45] and confidence masking [23, 56]. Combining it with newly found advanced augmentations, our Single-Network based approach can surpass the original Dual-Network [58] and come close to SSPCM using a Triple-Network. Our contributions are as follows:

- We comprehensively evaluated the difficulty levels of existing data augmentations suitable for the SSHPE task, validated their synergistic effects by properly combining different basic augmentations, and presented novel combination paradigms which are intuitively interpretable.
- We proposed to generate multi-path predictions of separately strongly augmented samples for training only one single model, rather than adding auxiliary networks. Thus, we can optimize multiple unsupervised losses efficiently and concisely, and benefit from distinct superior augmentations.
- We achieved new SOTA results on public SSHPE benchmarks with less training time and parameters under same settings of previous methods.

2 Related Work

Semi-Supervised Learning (SSL). SSL is invented for improving the classification task by exploiting a small set of labeled data and a large set of unlabeled data. It can be categorized into pseudo-label (PL) based [16, 40, 45, 47, 52, 57] and consistency-based [3, 14, 15, 27, 50, 56, 67]. PL-based methods iteratively add unlabeled images into the training data by pseudo-labeling them with a pre-trained or gradually enhanced model. It needs to find suitable thresholds to mask out uncertain samples with low-confidence, which is a crucial yet tricky issue. Consistency-based methods enforce model outputs to be consistent when its input is randomly perturbed. They have shown to work well on many tasks. For example, MixMatch [3] combines the consistency regularization with the entropy minimization to obtain confident predictions. FixMatch [47] utilizes a weak-to-strong consistency regularization and integrates the pseudo-labeling to leverage unlabeled data. FlexMatch [67] and FreeMatch [52] adopt the curriculum learning and adaptive thresholding based on FixMatch, respectively. CRMATCH [14] and SAA [15] try to design strategies and augmentations to enhance the consistency training. These SSL methods give us primitive inspirations.

Semi-Supervised Human Pose Estimation (SSHPE). The SSHPE task is relatively less-studied comparing to other visual tasks such as classification and object detection. A few representative methods are based on pseudo labeling [48, 51] or consistency training [23, 28, 37, 58]. SSKL [37] designs a semantic keypoint consistency constraint to learn invariant representations of same keypoints. It has been evaluated on small-scale HPE benchmarks MPII [1] and LSP [24], instead of the larger COCO [34]. Following it, PLACL [51] introduces the curriculum learning by auto-selecting dynamic thresholds for producing pseudo-labels via reinforcement learning. Inspired by co-training [44] and dual-student [26], Dual-Network [58] points out the typical collapsing problem in SSHPE, and proposes the easy-hard augmentation pair on the same input to imitate teacher-student signals without relying on Mean Teacher [50]. SSPCM [23] extends the Dual into Triple by adding an auxiliary teacher for interactive training in multi-steps. It designs a handcrafted pseudo-label correction based on the predicted position inconsistency of two teachers, and has achieved SOTA performances. We revisit the less efficient-consistency training way in [23, 58], and propose to upgrade the Single-Network furtherly by multi-path predictions.

Unsupervised Data Augmentations. The UDA [56] has emphasized and verified the key role of high-quality noise injection (*e.g.*, data augmentations) in improving unsupervised consistency training. It utilizes advanced augmentations [10, 11] to promote the SSL classification. Then, [58] transfers the positive correlation between strong augmentations and SSL performance to the HPE field. It introduces a more advanced augmentation called Joint Cutout inspired by Cutout [12]. Similarly, SSPCM [23] provides a harder keypoints-sensitive augmentation Cut-Occlude inherited from CutMix [66]. In this paper, we thoroughly revisit existing data augmentations suitable to SSHPE, give a rank of their difficulty levels by controlled trainings, and produce simple paradigms for getting novel superior joint-related augmentations. We also compare them with other well-designed counterparts [11, 17, 38] to reveal our advantages.

3 Empirical Studies

Problem Definition: The task of 2D HPE is to detect k body joints in an image $\mathbf{I} \in \mathbb{R}^{h \times w \times 3}$. The state-of-the-art methods tend to estimate k Gaussian heatmaps $\mathbf{H} \in \mathbb{R}^{\frac{h}{s} \times \frac{w}{s} \times k}$ downsampled s times. For inference, each keypoint is located by finding the pixel with largest value in its predicted heatmap. We denote the labeled and unlabeled training sets as $\mathcal{D}^l = \{(\mathbf{I}_i^l, \mathbf{H}_i^l)\}_{i=1}^N$ and $\mathcal{D}^u = \{\mathbf{I}_i^u\}_{i=1}^M$, respectively. The \mathbf{H}^l are ground-truth heatmaps generated using 2D keypoints. For supervised training of the network f , we calculate the MSE loss:

$$\mathcal{L}_s = \mathbb{E}_{\mathbf{I} \in \mathcal{D}^l} \|f(T_e(\mathbf{I})) - T_e(\mathbf{H})\|^2 \quad (1)$$

where T_e represents an easy affine augmentation including a random rotation angle from $[-30^\circ, 30^\circ]$ and scale factor from $[0.75, 1.25]$ (denoted as T_{A30}). For unlabeled images, we calculate the unsupervised consistency loss:

$$\mathcal{L}_u = \mathbb{E}_{\mathbf{I} \in \mathcal{D}^u} \|T_{e \rightarrow h}(f(T_e(\mathbf{I}))) - f(T_h(\mathbf{I}))\|^2 \quad (2)$$

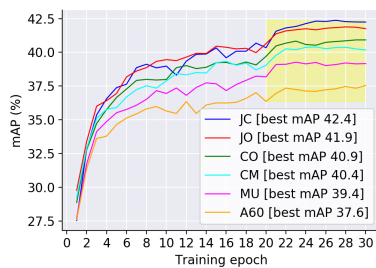


Fig. 2: Comparison of applying different easy-hard pairs for training a Single-Network model as in Fig. 1a. We can sort these six augmentations indisputably based on either best mAP results or distinct convergence curves.

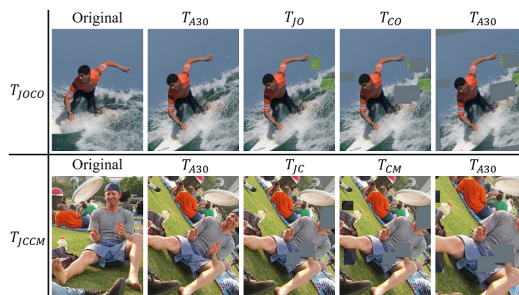


Fig. 3: Illustrations of two novel superior combinations T_{JOCO} and T_{JCCM} . Either of them is a sequential operations using ready-made collaborative augmentation. And T_{JO} and T_{CM} introduce extra patches cropped from other images which are not displayed.

where T_h is a harder augmentation with strong perturbations than affine-based T_e . The $T_{e \rightarrow h}$ means a known affine transformation on heatmaps if T_h contains additional rotation and scaling operations. In this way, we can obtain a paired *easy-hard* augmentations $(\mathbf{I}_e, \mathbf{I}_h) = (T_e(\mathbf{I}), T_h(\mathbf{I}))$ for generating corresponding teacher signals and student signals. During training, we should stop gradients propagation of teacher signals to avoid collapsing.

Next, we answer two questions Q1 and Q2 by extensive empirical studies in Sec. 3.1 and Sec. 3.2, respectively. After that, we provide a perspective for understanding the pursuit of strong augmentations in Sec. 3.3.

3.1 Paradigms of Generating Superior Augmentations

Ranking of Basic Augmentations. The core of the easy-hard pair paradigm $(\mathbf{I}_e, \mathbf{I}_h)$ is a more advanced augmentation. For this reason, Dual-Network [58] and SSPCM [23] propose pseudo keypoint-based augmentations Joint Cutout (T_{JC}) and Joint Cut-Occlude (T_{JO}), respectively. They also reach a similar yet crude conclusion about difficulty levels of existing augmentations: $\{T_{JO}, T_{JC}\} > \{T_{RA}, T_{CM}, T_{CO}, T_{MU}, T_{A60}\}$, where T_{RA} , T_{CM} , T_{CO} and T_{MU} are RandAugment [11], CutMix [66], Cutout [12] and Mixup [70], respectively. The T_{A60} consists of two T_{A30} . We give them a new ranking by conducting more rigorous trainings one-by-one. The T_{RA} is removed for it contains repetitions with T_{CO} and T_{A60} . As shown in Fig. 2, we divide the rest by their distinguishable gaps into four levels: $\{T_{JC}, T_{JO}\} > \{T_{CO}, T_{CM}\} > \{T_{MU}\} > \{T_{A60}\}$.

Synergy between Augmentations. Then, instead of laboriously designing stronger augmentations, we consider to conduct two or more augmentations in sequence to obtain superior combinations conveniently. This idea is feasible because it essentially belongs to the AutoAug families [10, 18, 33, 72]. Instead of auto-searching, we expect to find some heuristic strategies for the HPE task. In fact, after performing joint-related T_{JO} or T_{JC} on one image, we can continue to perform some joint-unrelated augmentations such as T_{CM} , T_{CO} and T_{MU} on

random areas. As shown in Fig. 3, applying T_{JOCO} (a T_{CO} after T_{JO}) or T_{JCCM} (a T_{CM} after T_{JC}) will bring harder samples for generating more effective student signals, but not destroy the semantic information visually. We call this discovery the **synergistic effect** between different augmentations. The T_{A60} can server as an essential factor in any T_h for keeping the geometric diversity.

Selection of Augmentations Combination. Now, if selecting from the rest five basic augmentations, there are up to 26 choices ($2^5 - \binom{5}{0} - \binom{5}{1}$). The optimal combinations are still time-consuming to acquire. Fortunately, not arbitrary number or kind of augmentations are collaborative. We intuitively summarize three simplistic principles. (P1) A global T_{MU} does not make sense for the HPE task. (P2) Stacking augmentations with the similar perturbation type (e.g., $T_{JO} \sim T_{CM}$ and $T_{JC} \sim T_{CO}$) or difficulty level (e.g., $T_{JO} \sim T_{JC}$ and $T_{CM} \sim T_{CO}$) may not bring significant gain. (P3) Adding too many augmentations (e.g., three or four) will be profitless or even harmful for seriously polluting the image. We thus nominate the most likely superior combinations: T_{JOCO} and T_{JCCM} . A case of setting T_e as T_{A30} and T_h as T_{JOCO} for getting corresponding easy teacher signals \mathbf{H}_e and hard student signals \mathbf{H}_h is shown as below:

$$\begin{aligned} \mathbf{H}_e &= T_{A30 \rightarrow A60}(f(\mathbf{I}_e)), \quad \mathbf{I}_e = T_{A30}(\mathbf{I}) \\ \mathbf{H}_h &= f(\mathbf{I}_h), \quad \mathbf{I}_h = T_{A30}(T_{CO}(T_{JO}(T_{A30}(\mathbf{I})))) \end{aligned} \quad (3)$$

where T_{A60} is default to T_h , and divided into two separate T_{A30} for being compatible with T_e . To further verify the above intuitive principles, we follow the augmentations ranking way and conduct empirical studies on the performance of up to 13 selected representative combinations out of 26 choices.

Table 1: Best mAP results of different combinations tests.

Id	Combination	mAP
-	T_{JC}	42.4
-	T_{JO}	41.9
c_1	$T_{JC,CM}$	42.7
c_2	$T_{JO,CO}$	43.7
c_3	$T_{JC,MU}$	41.8
c_4	$T_{JO,MU}$	42.1
c_5	$T_{JC,CO}$	42.1
c_6	$T_{JO,CM}$	42.5
c_7	$T_{JC,JO}$	42.0
c_8	$T_{JC,CM,MU}$	42.0
c_9	$T_{JO,CO,MU}$	42.8
c_{10}	$T_{JC,JO,CO}$	41.7
c_{11}	$T_{JC,JO,CM}$	42.3
c_{12}	$T_{JC,CO,CM}$	42.8
c_{13}	$T_{JO,CO,CM}$	42.8

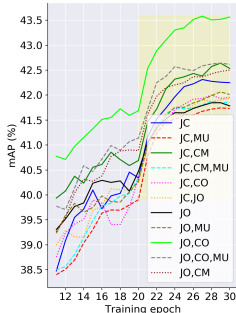


Fig. 4: The convergence curves of different tests in Tab. 1.

Table 2: Best mAP results of different MultiAugs tests.

Id	MultiAugs	mAP
m_1	T_{JC}, T_{CM}	43.0
m_2	T_{JO}, T_{CO}	43.4
m_3	T_{JC}, T_{JO}	43.1
m_4	T_{JCCM}, T_{CO}	43.7
m_5	T_{JOCO}, T_{CM}	43.1
m_6	T_{JOCO}, T_{JC}	44.2
m_7	T_{JCCM}, T_{JO}	42.9
m_8	$T_{JC}, T_{JO}, T_{CO}, T_{CM}$	43.6
m_9	T_{JCCM}, T_{JCCM}	43.6
m_{10}	T_{JOCO}, T_{JOCO}	44.0
m_{11}	T_{JOCO}, T_{JCCM}	44.9
m_{12}	$T_{JOCO}, T_{JC}, T_{JCCM}, T_{JO}$	45.5

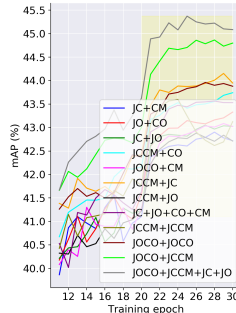


Fig. 5: The convergence curves of different tests in Tab. 2.

As shown in Tab. 1 and Fig. 4, we can examine three principles one-by-one: (P1) T_{MU} often causes adverse or inferior effects for each combination. Please refer paired combinations c_1 - c_3 , c_2 - c_4 , c_1 - c_8 and c_2 - c_9 . Thus, we do not add it for finding superior combinations. (P2) Synergistic effects between augmentations do exist. Please refer paired combinations c_1 - c_5 , c_1 - c_7 , c_2 - c_6 and c_2 - c_7 . Especially, the T_{JCJO} with two most advanced augmentations performs the worst among combinations $\{c_1, c_2, c_5, c_6, c_7\}$, which roundly reveals the harm of violating the principle of synergy. (P3) Do not overly combine too many augmentations. Please

refer paired combinations c_1-c_{12} , c_2-c_{13} , c_1-c_{11} and c_2-c_{10} . Stacking more augmentations brings non-significant gains or even results in degradation. We attribute it to deviating from the rule of collaboration and possibly producing meaningless or difficult-to-recognize images. Based on these facts, we have sufficient reasons not to check the performance of rest combinations. And we recommend two new strongest combinations T_{JOCO} and T_{JCCM} .

3.2 Multi-path Consistency Losses

To further amplify the advantage of easy-hard augmentation, [58] adopts two independent networks containing two easy-hard pairs for producing two consistency losses. SSPCM [23] continues this route by designing a Triple-Network with three easy-hard pairs. Meanwhile, some SSL methods construct multi-view inputs for unlabeled data without adding accompanying networks. For example, SwAV [5] enforces the local-to-global consistency among a bag of views with different resolutions. ReMixMatch [2] feeds multiple strongly augmented versions of an input into the model for training. Therefore, we wonder whether such a simple idea can also benefit the SSHPE task.

Specifically, rather than feeding a single hard augmentation \mathbf{I}_h into the model, we independently yield n strongly augmented inputs $\mathcal{I}^n = \{\mathbf{I}_{h_1}, \mathbf{I}_{h_2}, \dots, \mathbf{I}_{h_n}\}$ from \mathbf{I} by applying n hard data augmentations $\mathcal{T}^n = \{T_{h_1}, T_{h_2}, \dots, T_{h_n}\}$ accordingly. The augmentation set \mathcal{T}^n is de-emphasized in order and non-deterministic, and will generate distinct multi-path augmented inputs \mathcal{I}^n . Then, we can calculate n -stream heatmaps $\mathcal{H}^n = \{f(T_{h_i}(\mathbf{I}_{h_i}))\}_{i=1}^n$. This multi-path augmentation framework is illustrated in Fig. 7. For regularizing n easy-hard pairs, we obtain multi-path consistency losses using Eq. 2 in separate, and optimize them jointly by applying multi-loss learning:

$$\mathcal{L}_u^* = \mathbb{E}_{\mathbf{H}_{h_i} \in \mathcal{H}^n} \sum_{i=1}^n \|\mathbf{H}_e - \mathbf{H}_{h_i}\|^2 \quad (4)$$

where \mathbf{H}_e and \mathbf{H}_{h_i} are obtained as dissected in Eq. 3. The \mathbf{H}_e keeps constant for each \mathbf{H}_{h_i} . Comparably, Data Distill [45] applies a single model to multiple transformations of unlabeled data to train a student model. Then, it ensembles predictions to obtain keypoint locations, and re-generates a pseudo heatmap for supervision. Differently, we argue that conducting a fusion on predicted heatmaps in SSHPE is harmful. We consider that there are always differences in the estimation of keypoint positions for each \mathbf{I}_{h_i} . It is an ill-posed problem to heuristically evaluate the consistency regularization contribution of each heatmap in pixel during ensemble. We will explain this in ablation studies Sec. 5.4.

Despite the simplicity, such a minor modification brings consistent gains over the original Single-Network under same SSL settings. With our discovered augmentation combinations T_{JOCO} and T_{JCCM} , the boosted Single-Network can surpass the original Dual-Network evidently. We validated in ablation studies that the performance gain is non-trivial. We conjecture that regularizing multiple hard augmentations with a shared easy augmentation can be regarded as enforcing consistency among advanced augmentations as well, which inherits

the concept of training positive-negative paired samples in contrastive learning [6, 7, 19] and its SSL-related variations [30, 54, 62].

Effectiveness Verification. As shown in Tab. 2 and Fig. 5, we also experimentally verified the major advantage of the multi-path augmentations (dubbed as MultiAugs) strategy. Here, we have two variables of MultiAugs: the number of paths and the category of augmentations. For acquisition of an optimal augmentations set, similarly, we continue with the rules summarized in the previous section, and elect 12 different MultiAugs schemes for illustrating. We can witness the effectiveness of MultiAugs from two aspects: (1) *It can inherit and even expand the synergistic effects between different augmentations.* (2) *It can alleviate the defects caused by excessive stacking of augmentations.*

Specifically, by comparing c_1 - m_1 , c_2 - m_2 and c_7 - m_2 , we find that MultiAugs provides comparable performance with the same augmentations. By comparing c_{10} - m_6 , c_{11} - m_7 , c_{12} - m_4 and c_{13} - m_5 , we can observe the sustained large gains brought by MultiAugs. The scheme m_8 does not obtain a better result than m_{11} showing that new augmentations T_{JOCO} and T_{JCCM} have their essential properties. Schemes m_9 and m_{10} which utilize a single augmentation twice are also inferior to m_{11} showing the cooperativity of using multi-path distinct augmentations. Moreover, the optimal scheme m_{12} further unleashes capabilities of four advanced augmentations. In order to balance performance and time consumption, we do not add more augmentation paths.

3.3 Analysis of Superior Augmentations

In this part, we tentatively analyze why employing a superior augmentation to strongly augment the unlabeled data can improve model performance. Different from UDA [56] using the improved connectivity of constructed graphs to explain, we start from the perspective of shaped feature space of unlabeled data based on the singular value spectrum, which is widely considered to be related to the model transferability and generalization [8, 60]. Specifically, we perform singular value decomposition (SVD) on features $\mathbf{F} \in \mathbb{R}^{N \times D}$ ³ extracted by various trained models with different strong augmentations on one dataset: $\mathbf{F} = \mathbf{U}\mathbf{\Sigma}\mathbf{V}^T$, where \mathbf{U} and \mathbf{V} is the left and right singular vector matrices, respectively, and $\mathbf{\Sigma}$ denotes the diagonal singular value matrix $\{\sigma_1, \sigma_2, \dots, \sigma_D\}$.

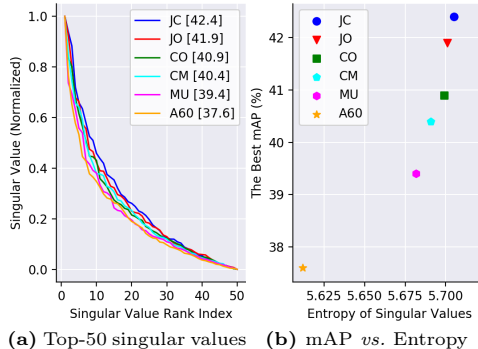


Fig. 6: SVD analysis. The backbone of all six models is ResNet18. The 512-D features of 6,352 samples in COCO *val-set* are extracted.

³ We denote N as the number of samples and D as feature dimensions (*a.k.a.*, $D \leq N$).

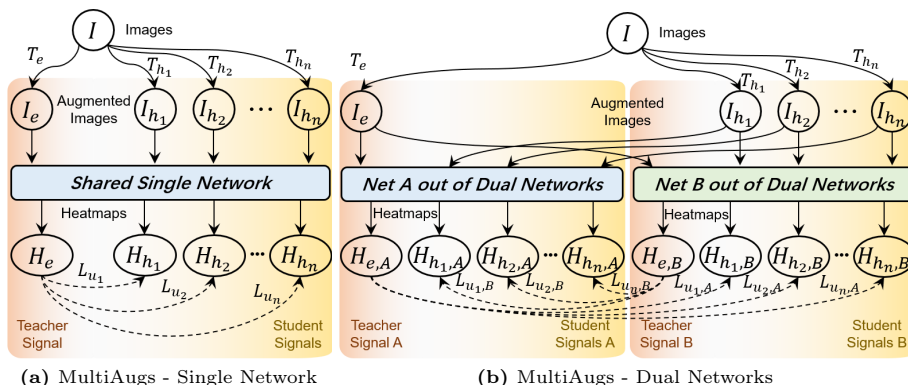


Fig. 7: Our MultiAugs uses the Single Network (a) or Dual Networks (b), which can utilize multiple hard augmentations and facilitate multi-path consistency training.

Then, we plot calculated singular values in Fig. 6a. To further measure the flatness of the singular value distribution, we calculate the entropy of normalized singular values H_{nsv} :

$$H_{nsv} = - \sum_{i=1}^D \frac{\sigma_i}{\sum_{j=1}^D \sigma_j} \log \frac{\sigma_i}{\sum_{j=1}^D \sigma_j} \quad (5)$$

Usually, a larger H_{nsv} indicates that the feature space captures more structure in the data and thus spans more dimensions due to more discriminated representations learned. As shown in Fig. 6b, the model performance is *positively correlated* with the H_{nsv} value. Therefore, a superior augmentation facilitates better model generalization to unseen test sets.

4 Our Overall Framework: MultiAugs

We leverage unlabeled images by applying multiple augmentations with integrating two key techniques introduced in Sec. 3.1 and Sec. 3.2. Firstly, assuming that we have obtained an optimal augmentation set $\hat{\mathcal{T}}^n = \{\hat{T}_{h_i} |_{i=1}^n\}$, where \hat{T}_{h_i} may be an old single augmentation or a novel combined one. Then, we present how to construct our overall training framework in Fig. 7 based on either the Single-Network or the Dual-Network.

MultiAugs (Single-Network). It is a consistency-based approach. We only need to maintain a single model as in Fig. 7a during training. For each input batch with equal number of labeled images \mathbf{I}^l and unlabeled images \mathbf{I}^u , we calculate the supervised loss with the ground-truth heatmaps as in Eq. 1, and the multiple unsupervised losses as in Eq. 4, respectively. The final loss is obtained by adding the two loss functions $\mathcal{L} = \mathcal{L}_s + \lambda \mathcal{L}_u^*$ with $\lambda = 1$. Note that we only pass the gradient back through n hard augmentations $\hat{\mathcal{T}}^n$ for generating teacher signals to avoid collapsing. Based on this boosted Single-Network, we complete all ablation experiments by changing the augmentation categories and quantities in $\hat{\mathcal{T}}^n$ for controlling the unsupervised factor \mathcal{L}_u^* .

MultiAugs (Dual-Network). As shown in Fig. 7b, this framework learns two identical yet independent networks with each similar to the Single-Network.

For one input batch in every step, each of the two networks serves as both a teacher and a student. They both are fed by easy and hard augmentations of unlabeled images \mathbf{I}^u when they produce teacher signals and student signals, respectively. Assuming we have two networks f_A and f_B , and also the augmented easy images \mathbf{I}_e^u using T_e and n -path hard images $\{\mathbf{I}_{h_1}^u, \mathbf{I}_{h_2}^u, \dots, \mathbf{I}_{h_n}^u\}$ using $\widehat{\mathcal{T}}^n$, we first predict the following four types of heatmaps:

$$\begin{aligned} \mathbf{H}_{e,A} &= T_{A30 \rightarrow A60}(f_A(\mathbf{I}_e^u)), & \mathcal{H}_A &= \{\mathbf{H}_{h_i,A}|_{i=1}^n, \mathbf{H}_{h_i,A} = f_A(\mathbf{I}_{h_i}^u)\} \\ \mathbf{H}_{e,B} &= T_{A30 \rightarrow A60}(f_B(\mathbf{I}_e^u)), & \mathcal{H}_B &= \{\mathbf{H}_{h_i,B}|_{i=1}^n, \mathbf{H}_{h_i,B} = f_B(\mathbf{I}_{h_i}^u)\} \end{aligned} \quad (6)$$

where $T_{A30 \rightarrow A60}$ is a pre-generated affine transformation. Based on above heatmaps, we calculate two unsupervised losses for training two networks as follows:

$$\begin{aligned} \mathcal{L}_{u,A}^* &= \mathbb{E}_{\mathbf{H}_{h_i,A} \in \mathcal{H}_A} \sum_{i=1}^n \|\mathbf{H}_{e,B} - \mathbf{H}_{h_i,A}\|^2 \\ \mathcal{L}_{u,B}^* &= \mathbb{E}_{\mathbf{H}_{h_i,B} \in \mathcal{H}_B} \sum_{i=1}^n \|\mathbf{H}_{e,A} - \mathbf{H}_{h_i,B}\|^2 \end{aligned} \quad (7)$$

where we swap positions of teacher signals $\mathbf{H}_{e,A}$ and $\mathbf{H}_{e,B}$ for realizing the cross training of networks f_B and f_A . Following [58], we report the average accuracy of the final two well-trained and performance-approached models. Besides, f_A and f_B can have different structures as in [23, 58], where the large one often helps to distill a better small model, but not vice versa. We do not intend to explore this consensus anymore in this paper.

5 Experiments

5.1 Datasets and Metrics

COCO. The dataset COCO [34] has 4 subsets: *train-set* (118K images), *val-set* (5K images), *test-dev* and *test-challenge*. It is a popular large-scale benchmark for human pose estimation, which contains over 150K annotated people. In addition, there are 123K wild unlabeled images (*wild-set*). We randomly selected 1K, 5K and 10K labeled data from *train-set*. In some experiments, unlabeled data came from the remaining images of *train-set*. In other experiments, we used the whole *train-set* as the labeled dataset and *wild-set* as the unlabeled dataset. The metric of mAP (Average AP over 10 OKS thresholds) is reported.

MPII and AI-Challenger. The dataset MPII [1] has 25K images and 40K person instances with 16 keypoints. The dataset AI-Challenger (AIC) [53] *train-set* has 210K images and 370K person instances with 14 keypoints. We use MPII as the labeled set, AIC as the unlabeled set. The metric of PCKh0.5 is reported.

5.2 Implementation Details

For a fair comparison with prior works, we use SimpleBaseline [55] to estimate heatmaps and ResNet [20] and HRNet [49] as backbones. The input image size is set to 256×192 . We adopt the PyTorch 1.30 and 4 A100 GPUs with each batch size as 32 for training. The initial learning rate is 1e-3. When training

on COCO with 10K labeled data, it decreases to $1e-4$ and $1e-5$ at epochs 70 and 90, respectively, with a total of 100 epochs. When using 1K or 5K labeled data, total epochs are reduced to 30 or 70, respectively. When training on the complete COCO or MPII+AIC, it drops to $1e-4$ and $1e-5$ at epochs 220 and 260, respectively, with a total of 300 epochs. When testing, we do not flip horizontally.

For data augmentation settings, we keep the easy augmentation T_e as T_{A30} in all experiments. The hard augmentations set $\hat{\mathcal{T}}^4 = \{T_{JOCO}, T_{JCCM}, T_{JC}, T_{JO}\}$ is chosen for the comparison **C1**. While, the less optimal augmentations set $\hat{\mathcal{T}}^2 = \{T_{JOCO}, T_{JCCM}\}$ is chosen for comparisons **C2**, **C3**, **C4** and **C5** to balance the performance and training time. We present details of finding two novel superior hard augmentations T_{JOCO} and T_{JCCM} , and selecting the optimal augmentation set $\hat{\mathcal{T}}^4$ in ablation studies.

5.3 Performance Comparison

Table 3: AP of different methods on COCO *val-set* when different numbers of labels are used. Backbone is ResNet18.

Method	Net. Num.	1K	5K	10K	All
Supervised [55]	1	31.5	46.4	51.1	67.1
PseudoPose [58]	2	37.2	50.9	56.0	—
DataDistill [45]	2	37.6	51.6	56.6	—
PoseCons [58]	1	42.1	52.3	57.3	—
PoseDual [58]	2	44.6	55.6	59.6	—
SSPCM [23]	3	46.9	57.5	60.7	—
Ours (Single)	1	45.5	56.2	59.9	—
Ours (Dual)	2	49.7	58.8	61.8	—

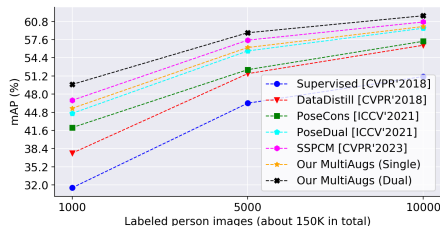


Fig. 8: Comparison between state-of-the-art SSHPE methods and our proposed MultiAugs on the COCO dataset.

We mainly compare our MultiAugs with representative SSHPE methods PoseDual [58] and SSPCM [23] under five conditions:

C1: Firstly, we conduct experiments on the COCO *train-set* with 1K, 5K and 10K labeled data, and evaluate on the *val-set*. As shown in Tab. 3 and Fig. 8, our method brings substantial improvements under the same setting. For example, when using a Single-Network, our method exceeds both PoseCons and PoseDual

Table 4: Results on the COCO *val-set* when labeled images from the *train-set* and unlabeled images from the *wild-set*.

Method	Backbone	Networks	AP	AP _{.5}	AR	AR _{.5}
Supervised [55]	ResNet50	Single	70.9	91.4	74.2	92.3
PoseDual [58]	ResNet50	Dual	73.9	92.5	77.0	93.5
SSPCM [23]	ResNet50	Triple	74.2	92.7	77.2	93.8
Ours (Single)	ResNet50	Single	74.0	92.5	77.1	93.9
Ours (Dual)	ResNet50	Dual	74.6	93.5	77.6	94.0
Supervised [55]	ResNet101	Single	72.5	92.5	75.6	93.1
PoseDual [58]	ResNet101	Dual	75.3	93.6	78.2	94.1
SSPCM [23]	ResNet101	Triple	75.5	93.8	78.4	94.2
Ours (Single)	ResNet101	Single	75.4	93.4	78.4	94.1
Ours (Dual)	ResNet101	Dual	76.3	93.5	79.2	94.4
Supervised [55]	HRNet-w48	Single	77.2	93.5	79.9	94.1
PoseDual [58]	HRNet-w48	Dual	79.2	94.6	81.7	95.1
SSPCM [23]	HRNet-w48	Triple	79.4	94.8	81.9	95.2
Ours (Single)	HRNet-w48	Single	79.3	94.6	81.8	95.1
Ours (Dual)	HRNet-w48	Dual	79.5	94.6	82.1	95.2

Table 5: Comparison to the SOTA methods on the COCO *test-dev*. The COCO *train-set* is the labeled set and COCO *wild-set* is the unlabeled set. The person detection results are provided by SimpleBaseline and flipping strategy is used.

Method	Backbone	Input Size	GFLOPS	#Params	AP	AR
SimpleBaseline [55]	ResNet50	256×192	8.9	34.0	70.2	75.8
HRNet [49]	HRNet-w48	384×288	32.9	63.6	75.5	80.5
MSPN [31]	ResNet50	384×288	58.7	71.9	76.1	81.6
DARK [68]	HRNet-w48	384×288	32.9	63.6	76.2	81.1
UDP [22]	HRNet-w48	384×288	33.0	63.8	76.5	81.6
TransPose-H-A6 [64]	HRNet-w48	256×192	21.8	17.5	75.0	—
TokenPose-L/D24 [32]	HRNet-w48	384×288	22.1	29.8	75.9	80.8
HRFormer [65]	HRFormer-B	384×288	26.8	43.2	76.2	81.2
ViTPose [59]	ViT-Large	256×192	59.8	307.0	77.3	—
DUAL (+HRNet) [58]	HRNet-w48	384×288	65.8	127.2	76.7	81.8
DUAL (+DARK) [58]	HRNet-w48	384×288	65.8	127.2	77.2	82.2
SSPCM (+DARK) [23]	HRNet-w48	384×288	98.7	190.8	77.5	82.4
Ours (Dual) (+HRNet)	HRNet-w48	384×288	65.8	127.2	76.8	81.8
Ours (Dual) (+DARK)	HRNet-w48	384×288	65.8	127.2	77.3	82.3

Table 6: The results on the *val-set* of the MPII dataset. HRNet is trained only on the MPII *train-set*. The “*” means using extra labeled dataset AIC. The “+” means applying the model ensemble.

Method	Hea	Sho	Elb	Wri	Hip	Kne	Ank	Total
HRNet [49]	97.0	95.7	89.4	85.6	87.7	85.8	82.0	89.5
HRNet* [49]	97.4	96.7	92.1	88.4	90.8	88.6	85.0	91.7
PoseDual [58]	97.4	96.6	91.8	87.5	89.6	87.6	83.8	91.1
Ours (Dual)	97.3	96.8	91.7	87.5	90.3	88.6	84.6	91.4
Ours+ (Dual)	97.3	96.8	91.9	88.1	90.6	89.2	85.0	91.7

Table 7: Comparisons on the MPII *test-set* (PCKh0.5). We use HRNetW32 as the backbone. Input size is 256×256. The MPII and AIC (w/o labels) are used for training.

Method	Hea	Sho	Elb	Wri	Hip	Kne	Ank	Total
Newell <i>et al.</i> [39]	98.2	96.3	91.2	87.1	90.1	87.4	83.6	90.9
Xiao <i>et al.</i> [55]	98.5	96.6	91.9	87.6	91.1	88.1	84.1	91.5
Ke <i>et al.</i> [25]	98.5	96.8	92.7	88.4	90.6	89.4	86.3	92.1
Sun <i>et al.</i> [49]	98.6	96.9	92.8	89.0	91.5	89.0	85.7	92.3
Zhang <i>et al.</i> [69]	98.6	97.0	92.8	88.8	91.7	89.8	86.6	92.5
Xie <i>et al.</i> [58]	98.7	97.3	93.7	90.2	92.0	90.3	86.5	93.0
Huang <i>et al.</i> [23]	98.7	97.5	94.0	90.6	92.5	91.1	87.1	93.3
Ours (Dual)	98.8	97.6	94.1	90.3	92.4	91.1	87.2	93.4

significantly, and is close to the SSPCM based on three networks. When using a Dual-Network, our method exceeds previous SOTA results by **2.8** mAP, **1.3** mAP, and **1.1** mAP under 1K, 5K and 10K settings, respectively. Note that our method can bring greater gains with less labeled data (*e.g.*, 1K images), which further explains its efficiency and superiority.

C2: Then, we conduct larger scale SSHPE experiments on the complete COCO dataset by using *train-set* as the labeled dataset and *wild-set* as the unlabeled dataset. As shown in Tab. 4, regardless of using any backbone, our method can always improve all supervised baseline results, and bring more gains than two compared SSHPE methods [58] and [23] with using dual networks. When using a single network, our method is still superior to PoseDual [58], and fairly close to SSPCM [23] based on triple networks.

C3: Besides, we also report our results using HRNet-w48 on the COCO *test-dev* in Tab. 5. Our method can slightly outperform the PoseDual but fall behind the best SSHPE. We attribute it to our fewer training epochs and less parameters which may lead to weaker generalization. Besides, we can observe

that MultiAugs outperforms some burdensome transformer-based methods [32, 64, 65], which reveals the significance of rational utilization of unlabeled data.

C4: Finally, we allocate the MPII *train-set* as a labeled set and the whole AIC as an unlabeled set. This is a more realistic setting where labeled and unlabeled images are from different datasets. Tab. 6 shows results on the MPII *val-set*. Our method outperforms both the supervised HRNet [49] and semi-supervised PoseDual [58] by a large margin under the same backbone. It is worth noting that our semi-supervised MultiAugs with applying the model ensemble can even approach the supervised HRNet with using extra labeled AIC.

C5: Then, as shown in Tab. 7, our results on the MPII *test-set* surpass all those of previous fully supervised methods and two semi-supervised counterparts PoseDual and SSPCM. This further validates the effectiveness and superiority of our proposed method.

5.4 Ablation Studies

To further study our proposed MultiAugs, we conduct ablation experiments under the setting of COCO 1K with a total of 30 epochs. The learning rate drops $10\times$ twice separately at epochs 20 and 25. All studied models take ResNet18 as the backbone, and follow the Single-Network framework.

Table 8: Best mAP results of different augmentations on COCO *val-set*.

Augmentations	Year	mAP
T_{RA} [11]	CVPRW'2020	41.9
T_{TA} [38]	ICCV'2021	40.2
T_{YOCO} [17] (T_{RA})	ICML'2022	42.5
T_{YOCO} [17] (T_{TA})	ICML'2022	41.6
T_{JC} [58]	ICCV'2021	42.4
T_{JO} [23]	CVPR'2023	41.9
Ours (T_{JCCM})	—	42.7
Ours (T_{JOCCO})	—	43.7

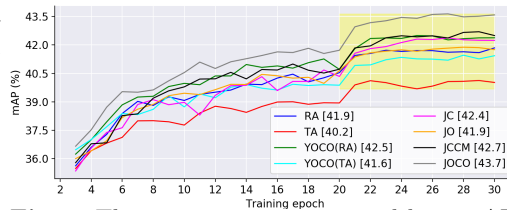


Fig. 9: The convergence curves and best mAP results of different strong augmentations.

Comparing to Other Advanced Augmentations. Three advanced augmentations are selected: RandAugment [11], TrivialAugment [38] and YOCO [17]. We refer to them as T_{RA} , T_{TA} and T_{YOCO} . For T_{YOCO} , it may be based on T_{RA} or T_{TA} . And we compare them with previous SOTA augmentations T_{JO} and T_{JC} for SSHPE, and our recommended T_{JOCCO} and T_{JCCM} . We did not compare to Mixup families [21, 36, 43, 70] or AutoAug families [10, 18, 33, 72]. Because Mixup is verified not to work with SSHPE, and AutoAug needs to search optimal parameters. Finally, as shown in Tab. 8 and Fig. 9, our optimal combinations are always better than T_{RA} -based or T_{TA} -based T_{YOCO} , which are meticulously designed and also composed of existing basic augmentations. These further prove the superiority and conciseness of our synergistic combinations.

Training Techniques of Multiple Heatmaps. In this part, we present additional techniques commonly used for unsupervised consistency training. Especially, for predicted multi-heatmaps, we propose to optimize them by applying the multi-loss learning (ML) as in Eq. 4. Other two alternative techniques are

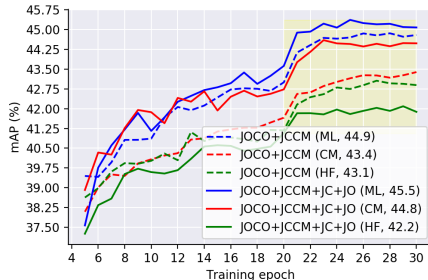


Fig. 10: The convergence curves and best mAP results of two MultiAugs schemes with using three different training techniques.

confidence masking (CM) and *heatmaps fusion* (HF). For CM, the consistency loss term in each mini-batch is computed only on keypoint channels whose maximum activation value is greater than a threshold τ , which is set as 0.5. For HF, also termed as *heatmaps ensemble*, we sum and average multi-path heatmaps to obtain a fused heatmap for loss computing. Then, we compare MultiAugs (e.g., m_{11} and m_{12}) using either of these three techniques ML, CM and HF.

As shown in Fig. 10, our ML is strictly superior than the other two techniques under either m_{11} or m_{12} . For CM, we assume it may filter out some keypoint heatmaps with low confidence but high quality. This surely has a negative impact. For HF, although it is widely used in other SSL tasks for model ensemble, it may not necessarily be applicable to our intermediate keypoint heatmaps. We deem this is because each predicted heatmap is distinctive and meaningful (see Fig. 11). It is tricky to replace them equivalently with a fused heatmap. In comparison, our multi-loss learning is a simple yet effective choice.

6 Conclusions

In this paper, we aim to boost semi-supervised human pose estimation (SSHPE) from two perspectives: data augmentation and consistency training. Instead of inventing advanced augmentations in isolation, we attempt to synergistically utilize existing augmentations, and handily generate superior ones by novel combination paradigms. The discovered collaborative combinations have intuitive interpretability. We verified their advantages in solving the SSHPE problem. For consistency training, we abandon the convention of stacking networks to increase unsupervised losses, and train a single network by optimizing multi-path consistency losses for the same batch of unlabeled images. Combined with the optimal hard augmentations set, this plain and compact strategy is proven to be effective, and leads to better performance on public benchmarks.

Last but not least, we declare that the synergy effects of augmentations and multiple consistency losses are generic and generalizable for other SSL vision tasks such as image classification, object detection and semantic segmentation. We will explore them in the future.

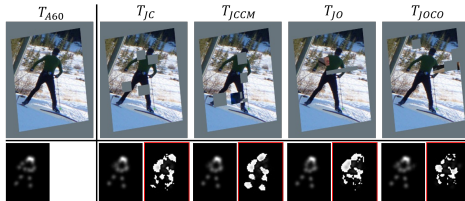


Fig. 11: The predicted heatmaps of one easy augmentation (T_{A60}) and four hard augmentations in m_{10} . We also report the pixel-wise heatmap difference (with red borders) of each easy-hard pair to highlight subtle dissimilarities.

References

1. Andriluka, M., Pishchulin, L., Gehler, P., Schiele, B.: 2d human pose estimation: New benchmark and state of the art analysis. In: Proceedings of the IEEE Conference on Computer Vision and Pattern Recognition. pp. 3686–3693 (2014) [1](#), [4](#), [10](#)
2. Berthelot, D., Carlini, N., Cubuk, E.D., Kurakin, A., Sohn, K., Zhang, H., Raffel, C.: Remixmatch: Semi-supervised learning with distribution matching and augmentation anchoring. In: International Conference on Learning Representations (2020) [7](#)
3. Berthelot, D., Carlini, N., Goodfellow, I., Papernot, N., Oliver, A., Raffel, C.A.: Mixmatch: A holistic approach to semi-supervised learning. *Advances in Neural Information Processing Systems* **32** (2019) [3](#)
4. Cao, Z., Simon, T., Wei, S.E., Sheikh, Y.: Realtime multi-person 2d pose estimation using part affinity fields. In: Proceedings of the IEEE Conference on Computer Vision and Pattern Recognition. pp. 7291–7299 (2017) [1](#)
5. Caron, M., Misra, I., Mairal, J., Goyal, P., Bojanowski, P., Joulin, A.: Unsupervised learning of visual features by contrasting cluster assignments. *Advances in Neural Information Processing Systems* **33**, 9912–9924 (2020) [7](#)
6. Chen, T., Kornblith, S., Norouzi, M., Hinton, G.: A simple framework for contrastive learning of visual representations. In: International Conference on Machine Learning. pp. 1597–1607. PMLR (2020) [8](#)
7. Chen, X., He, K.: Exploring simple siamese representation learning. In: Proceedings of the IEEE Conference on Computer Vision and Pattern Recognition. pp. 15750–15758 (2021) [8](#)
8. Chen, X., Wang, S., Long, M., Wang, J.: Transferability vs. discriminability: Batch spectral penalization for adversarial domain adaptation. In: International Conference on Machine Learning. pp. 1081–1090. PMLR (2019) [8](#)
9. Cheng, B., Xiao, B., Wang, J., Shi, H., Huang, T.S., Zhang, L.: Higherhrnet: Scale-aware representation learning for bottom-up human pose estimation. In: Proceedings of the IEEE Conference on Computer Vision and Pattern Recognition. pp. 5386–5395 (2020) [1](#)
10. Cubuk, E.D., Zoph, B., Mane, D., Vasudevan, V., Le, Q.V.: Autoaugment: Learning augmentation policies from data. *arXiv preprint arXiv:1805.09501* (2018) [3](#), [4](#), [5](#), [13](#)
11. Cubuk, E.D., Zoph, B., Shlens, J., Le, Q.V.: Randaugment: Practical automated data augmentation with a reduced search space. In: Proceedings of the IEEE Conference on Computer Vision and Pattern Recognition Workshops. pp. 702–703 (2020) [3](#), [4](#), [5](#), [13](#)
12. DeVries, T., Taylor, G.W.: Improved regularization of convolutional neural networks with cutout. *arXiv preprint arXiv:1708.04552* (2017) [3](#), [4](#), [5](#)
13. Duan, H., Zhao, Y., Chen, K., Lin, D., Dai, B.: Revisiting skeleton-based action recognition. In: Proceedings of the IEEE Conference on Computer Vision and Pattern Recognition. pp. 2969–2978 (2022) [1](#)
14. Fan, Y., Kukleva, A., Dai, D., Schiele, B.: Revisiting consistency regularization for semi-supervised learning. *International Journal of Computer Vision* **131**(3), 626–643 (2023) [3](#)
15. Gui, G., Zhao, Z., Qi, L., Zhou, L., Wang, L., Shi, Y.: Enhancing sample utilization through sample adaptive augmentation in semi-supervised learning. In: Proceedings of the IEEE International Conference on Computer Vision. pp. 15880–15889 (2023) [3](#)

16. Guo, L.Z., Li, Y.F.: Class-imbalanced semi-supervised learning with adaptive thresholding. In: International Conference on Machine Learning. pp. 8082–8094. PMLR (2022) [3](#)
17. Han, J., Fang, P., Li, W., Hong, J., Armin, M.A., Reid, I., Petersson, L., Li, H.: You only cut once: Boosting data augmentation with a single cut. In: International Conference on Machine Learning. pp. 8196–8212. PMLR (2022) [3](#), [4](#), [13](#)
18. Hataya, R., Zdenek, J., Yoshizoe, K., Nakayama, H.: Faster autoaugment: Learning augmentation strategies using backpropagation. In: European Conference on Computer Vision. pp. 1–16. Springer (2020) [3](#), [5](#), [13](#)
19. He, K., Fan, H., Wu, Y., Xie, S., Girshick, R.: Momentum contrast for unsupervised visual representation learning. In: Proceedings of the IEEE Conference on Computer Vision and Pattern Recognition. pp. 9729–9738 (2020) [8](#)
20. He, K., Zhang, X., Ren, S., Sun, J.: Deep residual learning for image recognition. In: Proceedings of the IEEE Conference on Computer Vision and Pattern Recognition. pp. 770–778 (2016) [10](#)
21. Hendrycks, D., Mu, N., Cubuk, E.D., Zoph, B., Gilmer, J., Lakshminarayanan, B.: Augmix: A simple data processing method to improve robustness and uncertainty. In: International Conference on Learning Representations (2020) [3](#), [13](#)
22. Huang, J., Zhu, Z., Guo, F., Huang, G.: The devil is in the details: Delving into unbiased data processing for human pose estimation. In: Proceedings of the IEEE Conference on Computer Vision and Pattern Recognition. pp. 5700–5709 (2020) [12](#)
23. Huang, L., Li, Y., Tian, H., Yang, Y., Li, X., Deng, W., Ye, J.: Semi-supervised 2d human pose estimation driven by position inconsistency pseudo label correction module. In: Proceedings of the IEEE Conference on Computer Vision and Pattern Recognition. pp. 693–703 (2023) [1](#), [2](#), [3](#), [4](#), [5](#), [7](#), [10](#), [11](#), [12](#), [13](#)
24. Johnson, S., Everingham, M.: Learning effective human pose estimation from inaccurate annotation. In: Proceedings of the IEEE Conference on Computer Vision and Pattern Recognition. pp. 1465–1472 (2011) [4](#)
25. Ke, L., Chang, M.C., Qi, H., Lyu, S.: Multi-scale structure-aware network for human pose estimation. In: Proceedings of the European Conference on Computer Vision. pp. 713–728 (2018) [12](#)
26. Ke, Z., Wang, D., Yan, Q., Ren, J., Lau, R.W.: Dual student: Breaking the limits of the teacher in semi-supervised learning. In: Proceedings of the IEEE International Conference on Computer Vision. pp. 6728–6736 (2019) [4](#)
27. Laine, S., Aila, T.: Temporal ensembling for semi-supervised learning. In: International Conference on Learning Representations (2016) [3](#)
28. Li, C., Lee, G.H.: Scarcenet: Animal pose estimation with scarce annotations. In: Proceedings of the IEEE Conference on Computer Vision and Pattern Recognition. pp. 17174–17183 (2023) [4](#)
29. Li, J., Wang, C., Zhu, H., Mao, Y., Fang, H.S., Lu, C.: Crowdpose: Efficient crowded scenes pose estimation and a new benchmark. In: Proceedings of the IEEE Conference on Computer Vision and Pattern Recognition. pp. 10863–10872 (2019) [1](#)
30. Li, J., Xiong, C., Hoi, S.C.: Comatch: Semi-supervised learning with contrastive graph regularization. In: Proceedings of the IEEE International Conference on Computer Vision. pp. 9475–9484 (2021) [8](#)
31. Li, W., Wang, Z., Yin, B., Peng, Q., Du, Y., Xiao, T., Yu, G., Lu, H., Wei, Y., Sun, J.: Rethinking on multi-stage networks for human pose estimation. arXiv preprint arXiv:1901.00148 (2019) [12](#)

32. Li, Y., Zhang, S., Wang, Z., Yang, S., Yang, W., Xia, S.T., Zhou, E.: Token-pose: Learning keypoint tokens for human pose estimation. In: Proceedings of the IEEE/CVF International Conference on Computer Vision. pp. 11313–11322 (2021) [12](#), [13](#)
33. Lim, S., Kim, I., Kim, T., Kim, C., Kim, S.: Fast autoaugment. *Advances in Neural Information Processing Systems* **32** (2019) [3](#), [5](#), [13](#)
34. Lin, T.Y., Maire, M., Belongie, S., Hays, J., Perona, P., Ramanan, D., Dollár, P., Zitnick, C.L.: Microsoft coco: Common objects in context. In: Proceedings of the European Conference on Computer Vision. pp. 740–755. Springer (2014) [1](#), [4](#), [10](#)
35. Liu, H., Chen, Q., Tan, Z., Liu, J.J., Wang, J., Su, X., Li, X., Yao, K., Han, J., Ding, E., et al.: Group pose: A simple baseline for end-to-end multi-person pose estimation. In: Proceedings of the IEEE International Conference on Computer Vision. pp. 15029–15038 (2023) [1](#)
36. Liu, Z., Li, S., Wu, D., Liu, Z., Chen, Z., Wu, L., Li, S.Z.: Automix: Unveiling the power of mixup for stronger classifiers. In: European Conference on Computer Vision. pp. 441–458. Springer (2022) [3](#), [13](#)
37. Moskvayak, O., Maire, F., Dayoub, F., Baktashmotlagh, M.: Semi-supervised keypoint localization. In: International Conference on Learning Representations (2021) [1](#), [4](#)
38. Müller, S.G., Hutter, F.: Trivialaugment: Tuning-free yet state-of-the-art data augmentation. In: Proceedings of the IEEE International Conference on Computer Vision. pp. 774–782 (2021) [3](#), [4](#), [13](#)
39. Newell, A., Yang, K., Deng, J.: Stacked hourglass networks for human pose estimation. In: Proceedings of the European Conference on Computer Vision. pp. 483–499. Springer (2016) [12](#)
40. Oliver, A., Odena, A., Raffel, C.A., Cubuk, E.D., Goodfellow, I.: Realistic evaluation of deep semi-supervised learning algorithms. *Advances in Neural Information Processing Systems* **31** (2018) [3](#)
41. Pavlakos, G., Choutas, V., Ghorbani, N., Bolkart, T., Osman, A.A., Tzionas, D., Black, M.J.: Expressive body capture: 3d hands, face, and body from a single image. In: Proceedings of the IEEE Conference on Computer Vision and Pattern Recognition. pp. 10975–10985 (2019) [1](#)
42. Pavlakos, G., Zhu, L., Zhou, X., Daniilidis, K.: Learning to estimate 3d human pose and shape from a single color image. In: Proceedings of the IEEE Conference on Computer Vision and Pattern Recognition. pp. 459–468 (2018) [1](#)
43. Pinto, F., Yang, H., Lim, S.N., Torr, P., Dokania, P.: Using mixup as a regularizer can surprisingly improve accuracy & out-of-distribution robustness. *Advances in Neural Information Processing Systems* **35**, 14608–14622 (2022) [3](#), [13](#)
44. Qiao, S., Shen, W., Zhang, Z., Wang, B., Yuille, A.: Deep co-training for semi-supervised image recognition. In: Proceedings of the European Conference on Computer Vision. pp. 135–152 (2018) [4](#)
45. Radosavovic, I., Dollár, P., Girshick, R., Gkioxari, G., He, K.: Data distillation: Towards omni-supervised learning. In: Proceedings of the IEEE Conference on Computer Vision and Pattern Recognition. pp. 4119–4128 (2018) [3](#), [7](#), [11](#)
46. Sarfraz, M.S., Schumann, A., Eberle, A., Stiefelhagen, R.: A pose-sensitive embedding for person re-identification with expanded cross neighborhood re-ranking. In: Proceedings of the IEEE Conference on Computer Vision and Pattern Recognition. pp. 420–429 (2018) [1](#)
47. Sohn, K., Berthelot, D., Carlini, N., Zhang, Z., Zhang, H., Raffel, C.A., Cubuk, E.D., Kurakin, A., Li, C.L.: Fixmatch: Simplifying semi-supervised learning with

- consistency and confidence. *Advances in Neural Information Processing Systems* **33**, 596–608 (2020) [3](#)
48. Springstein, M., Schneider, S., Althaus, C., Ewerth, R.: Semi-supervised human pose estimation in art-historical images. In: *Proceedings of the 30th ACM International Conference on Multimedia*. pp. 1107–1116 (2022) [4](#)
 49. Sun, K., Xiao, B., Liu, D., Wang, J.: Deep high-resolution representation learning for human pose estimation. In: *Proceedings of the IEEE Conference on Computer Vision and Pattern Recognition*. pp. 5693–5703 (2019) [1](#), [10](#), [12](#), [13](#)
 50. Tarvainen, A., Valpola, H.: Mean teachers are better role models: Weight-averaged consistency targets improve semi-supervised deep learning results. *Advances in Neural Information Processing Systems* **30** (2017) [3](#), [4](#)
 51. Wang, C., Jin, S., Guan, Y., Liu, W., Qian, C., Luo, P., Ouyang, W.: Pseudo-labeled auto-curriculum learning for semi-supervised keypoint localization. In: *International Conference on Learning Representations* (2022) [1](#), [4](#)
 52. Wang, Y., Chen, H., Heng, Q., Hou, W., Fan, Y., Wu, Z., Wang, J., Savvides, M., Shinozaki, T., Raj, B., et al.: Freematch: Self-adaptive thresholding for semi-supervised learning. In: *The Eleventh International Conference on Learning Representations* (2023) [3](#)
 53. Wu, J., Zheng, H., Zhao, B., Li, Y., Yan, B., Liang, R., Wang, W., Zhou, S., Lin, G., Fu, Y., et al.: Large-scale datasets for going deeper in image understanding. In: *2019 IEEE International Conference on Multimedia and Expo (ICME)*. pp. 1480–1485. *IEEE* (2019) [1](#), [10](#)
 54. Wu, J., Yang, H., Gan, T., Ding, N., Jiang, F., Nie, L.: Chmatch: Contrastive hierarchical matching and robust adaptive threshold boosted semi-supervised learning. In: *Proceedings of the IEEE Conference on Computer Vision and Pattern Recognition*. pp. 15762–15772 (2023) [8](#)
 55. Xiao, B., Wu, H., Wei, Y.: Simple baselines for human pose estimation and tracking. In: *Proceedings of the European Conference on Computer Vision*. pp. 466–481 (2018) [1](#), [10](#), [11](#), [12](#)
 56. Xie, Q., Dai, Z., Hovy, E., Luong, T., Le, Q.: Unsupervised data augmentation for consistency training. *Advances in Neural Information Processing Systems* **33**, 6256–6268 (2020) [3](#), [4](#), [8](#)
 57. Xie, Q., Luong, M.T., Hovy, E., Le, Q.V.: Self-training with noisy student improves imagenet classification. In: *Proceedings of the IEEE Conference on Computer Vision and Pattern Recognition*. pp. 10687–10698 (2020) [3](#)
 58. Xie, R., Wang, C., Zeng, W., Wang, Y.: An empirical study of the collapsing problem in semi-supervised 2d human pose estimation. In: *Proceedings of the IEEE International Conference on Computer Vision*. pp. 11240–11249 (2021) [1](#), [2](#), [3](#), [4](#), [5](#), [7](#), [10](#), [11](#), [12](#), [13](#)
 59. Xu, Y., Zhang, J., Zhang, Q., Tao, D.: Vitpose: Simple vision transformer baselines for human pose estimation. *Advances in Neural Information Processing Systems* **35**, 38571–38584 (2022) [1](#), [12](#)
 60. Xue, Y., Whitecross, K., Mirzasoleiman, B.: Investigating why contrastive learning benefits robustness against label noise. In: *International Conference on Machine Learning*. pp. 24851–24871. *PMLR* (2022) [8](#)
 61. Yan, S., Xiong, Y., Lin, D.: Spatial temporal graph convolutional networks for skeleton-based action recognition. In: *Proceedings of the AAAI Conference on Artificial Intelligence*. vol. 32 (2018) [1](#)
 62. Yang, F., Wu, K., Zhang, S., Jiang, G., Liu, Y., Zheng, F., Zhang, W., Wang, C., Zeng, L.: Class-aware contrastive semi-supervised learning. In: *Proceedings of the*

- IEEE Conference on Computer Vision and Pattern Recognition. pp. 14421–14430 (2022) [8](#)
63. Yang, J., Zeng, A., Liu, S., Li, F., Zhang, R., Zhang, L.: Explicit box detection unifies end-to-end multi-person pose estimation. *International Conference on Learning Representations (2023)* [1](#)
 64. Yang, S., Quan, Z., Nie, M., Yang, W.: Transpose: Keypoint localization via transformer. In: *Proceedings of the IEEE/CVF International Conference on Computer Vision*. pp. 11802–11812 (2021) [12](#), [13](#)
 65. Yuan, Y., Fu, R., Huang, L., Lin, W., Zhang, C., Chen, X., Wang, J.: Hrformer: High-resolution transformer for dense prediction. *Advances in Neural Information Processing Systems* **34**, 7281–7293 (2021) [12](#), [13](#)
 66. Yun, S., Han, D., Oh, S.J., Chun, S., Choe, J., Yoo, Y.: Cutmix: Regularization strategy to train strong classifiers with localizable features. In: *Proceedings of the IEEE International Conference on Computer Vision*. pp. 6023–6032 (2019) [3](#), [4](#), [5](#)
 67. Zhang, B., Wang, Y., Hou, W., Wu, H., Wang, J., Okumura, M., Shinozaki, T.: Flexmatch: Boosting semi-supervised learning with curriculum pseudo labeling. *Advances in Neural Information Processing Systems* **34**, 18408–18419 (2021) [3](#)
 68. Zhang, F., Zhu, X., Dai, H., Ye, M., Zhu, C.: Distribution-aware coordinate representation for human pose estimation. In: *Proceedings of the IEEE Conference on Computer Vision and Pattern Recognition*. pp. 7093–7102 (2020) [12](#)
 69. Zhang, H., Ouyang, H., Liu, S., Qi, X., Shen, X., Yang, R., Jia, J.: Human pose estimation with spatial contextual information. *arXiv preprint arXiv:1901.01760* (2019) [12](#)
 70. Zhang, H., Cisse, M., Dauphin, Y.N., Lopez-Paz, D.: mixup: Beyond empirical risk minimization. In: *International Conference on Learning Representations (2018)* [3](#), [5](#), [13](#)
 71. Zhao, H., Tian, M., Sun, S., Shao, J., Yan, J., Yi, S., Wang, X., Tang, X.: Spindle net: Person re-identification with human body region guided feature decomposition and fusion. In: *Proceedings of the IEEE Conference on Computer Vision and Pattern Recognition*. pp. 1077–1085 (2017) [1](#)
 72. Zheng, Y., Zhang, Z., Yan, S., Zhang, M.: Deep autoaugment. In: *International Conference on Learning Representations (2022)* [3](#), [5](#), [13](#)